Electronic Supplementary Material (ESI) for Environmental Science: Nano.

Supplementary Information

Effects of Rhamnolipid Biosurfactant on the Dissolution and Transport of Silver Nanoparticles in Porous Media

Shuchi Liao[1], Chen Liu[1], Dorothea Pinchbeck[1], Natalie L. Cápiro[2], John D. Fortner[3], Linda M. Abriola[1] and Kurt D. Pennell[1]*

[1] School of Engineering, Brown University, Providence, Rhode Island, 02912, United States
[2] Department of Civil Engineering, Environmental Engineering Program, Auburn University, Auburn, Alabama, 36849, United States

[3] Department of Chemical and Environmental Engineering, Yale University, New Haven, CT, 06520, United States

*Corresponding Author:
Kurt D. Pennell, PhD, PE, BCEE
School of Engineering, Brown University
Box D, 184 Hope Street
Providence, RI 02912
office: 401-863-9034
cell: 781-502-8545
Email: kurt_pennell@brown.edu

1. Non-reactive tracer tests

To characterize water flow and hydrodynamic dispersion, a non-reactive tracer test was conducted for each column experiment using a pH and DO concentration adjusted 10 mM NaBr

solution. Effluent bromide ion concentrations were measured using an Ion-Selective Electrode (Cole-Parmer, IL) and fit to a one-dimensional form of the advective-dispersive-reactive (ADR) transport equation using CXTFIT [1] ver 2.163 to obtain the hydrodynamic dispersion coefficient (D_H) and retardation factor (R_F), as shown in Figure S1. The fitted retardation factors are 0.99±0.02 and the dispersion coefficients ranged from 0.00027 to 0.00067 $cm^2\ s^{-1}$.

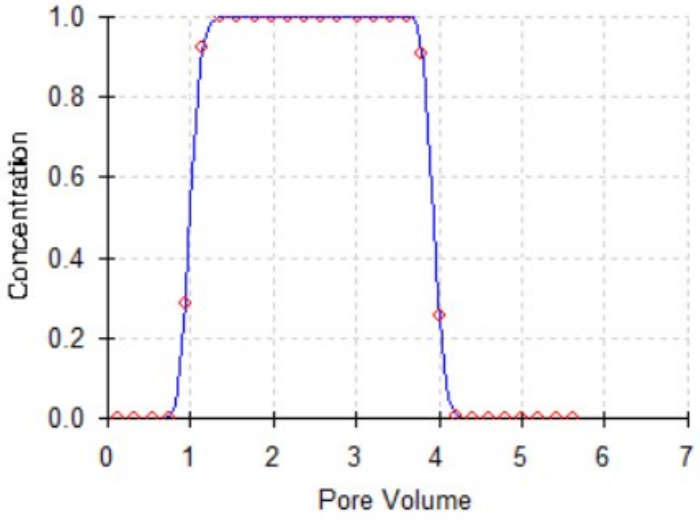

Figure S1. Representative experimental and fitted bromide tracer breakthrough curve.

2. nAg dissolution kinetics

Batch experiments were conducted to investigate dissolution kinetics of nAg in aqueous suspensions as a function of rhamnolipid concentration under three environmentally-relevant solution chemistries: 1) pH = 4.0±0.2 and DO = 8.8±0.2 mg L^{-1}, 2) pH = 7.0±0.2 and DO = 8.8±0.2 mg L^{-1}, 3) pH = 7.0±0.2 and DO = 2.0±0.2 mg L^{-1} . . Batch reactors were prepared by pH and DO adjustment, followed by nAg addition. Ag^+ concentration in batch reactors were monitored over 48 hours. The results for pH = 4.0±0.2 with DO = 8.8±0.2 mg L^{-1} are shown in Figure 1. The results for pH = 7.0±0.2 with DO = 8.8±0.2 mg L^{-1} and pH = 7.0±0.2 with DO = 2.0±0.2 mg L^{-1} are shown in Figures S2a-b and S2c-d, respectively.

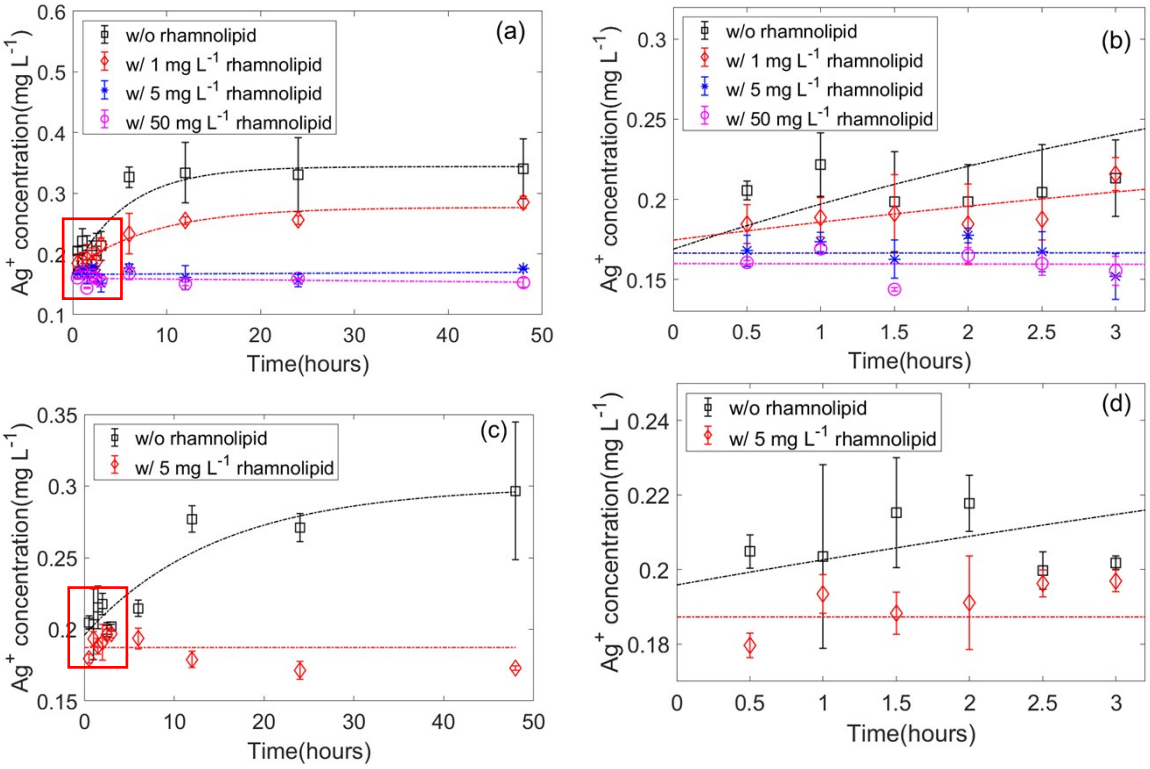

Figure S2. (a-b) nAg dissolution kinetics at pH 7.0±0.2 and dissolved oxygen concentration of 8.8±0.2 mg L^{-1} over 48 hours, early time data (first 3 h, in the red box) are enlarged in (b). (c-d) nAg dissolution kinetics at pH 4.0±0.2 and dissolved oxygen concentration of 2±0.2 mg L^{-1} over 48 hours, early time data (first 3 h, in the red box) are enlarged in (d). Data were fit to a first order dissolution kinetics equation. Error bars represent the standard deviation of duplicate or triplicate measurements.

Here, the first order silver nanoparticle dissolution kinetics developed by Zhang et al. [2] was modified to account for initial Ag^+ concentration in the nAg aqueous solution. The mathematical expression assumes passivation of surface dissolution sites:

$$\ln\left(1-\frac{C_w^{Ag^+}-C_w^{Ag^+,i}}{C_w^{Ag^+,max}}\right)=-k_d t \qquad (S1)$$

Where $C_w^{Ag^+,i}$ is the initial silver ion concentration in the solution, $C_w^{Ag^+,max}$ is the maximum dissolvable concentration of nAg, and k_d is the first order effective dissolution rate constant (h^{-1}). Assuming that nAg provides the only source of Ag^+, the following expression can be derived from equation S1 to calculate the Ag^+ concentration in the solution:

$$C_w^{Ag^+}=C_w^{Ag^+,max}\left(1-e^{-k_d t}\right)+C_w^{Ag^+,i} \qquad (S2)$$

The modified first-order model assumes that only a limited number of silver nanoparticle surface sites are available for dissolution during a given time frame. The model was fit to experimental data using a Matlab nonlinear least square procedure (MATLAB, R2020a).

Three model parameters, including maximum dissolvable concentration $C^{Ag^+,max}_w$, effective dissolution rate constant k_d and initial Ag ion concentration $C^{Ag^+,i}_w$, were fit. The initial Ag ion concentration could not be measured directly since at least 20 mins of centrifugation is needed to separate the ions from the solution after the batch experiments begin. Therefore, the data start from time = 0.5 hours and the $C^{Ag^+,i}_w$ was fitted in this study.

The relatively high values and variations in fitted $C^{Ag^+,i}_w$ can be attributed to a number of factors: 1) During storage, it is likely that silver ions slowly released from nAg and absorbed on nAg surfaces [3]. Once diluted, this absorbed Ag^+ could be desorbed from the surface quickly. The batch experiments were conducted and repeated over a period of 2 months and longer storage times resulted in more surface-absorbed Ag^+, leading to higher and varied initial Ag^+ concentrations. 2)Similarly, Ag_2O layers would also gradually form on the nAg surfaces during storage, which then could dissolve rapidly under low pH onditions, and result in higher initial concentrations for all pH 4 batches.

Table S1. Batch experimental conditions (pH, DO, and Rhamnolipid concentration) and corresponding nAg dissolution parameters (maximum dissolvable concentration $C^{Ag^+,max}_w$, effective dissolution rate constant k_d and initial Ag ion concentration $C^{Ag^+,i}_w$). The parameters were obtained by fitting batch experimental results to the first order nAg dissolution kinetics (Equation S2).

pH	DO	Rham.Conc (mg L^{-1})	$C^{Ag^+,max}_w$ (mg L^{-1})	k_d(h^{-1})	$C^{Ag^+,i}_w$ (mg L^{-1})
4	8.8	0	0.6526	0.0537	0.3331
4	8.8	1	0.4553	0.0701	0.2947
4	8.8	2	0.1134	0.1448	0.3066
4	8.8	5	0.1015	0.0168	0.2806
4	8.8	50	0.0467	0.0552	0.2593
7	8.8	0	0.1751	0.1755	0.1689
7	8.8	1	0.1022	0.1162	0.1746
7	8.8	5	0†	0.0000	0.1666
7	8.8	50	0†	0.0002	0.1599
7	2.0	0	0.1042	0.0669	0.1959

7	2.0	5	0.0000	0.0000	0.1873

†The fitted values in these cases are negative numbers which are close to 0, given $C_{w}^{Ag^{+},max} \geq 0$, here take 0 as fitted values instead.

3. nAg aggregation kinetics at pH = 7 and DO = 8.8 or 2.0 mg L^{-1}

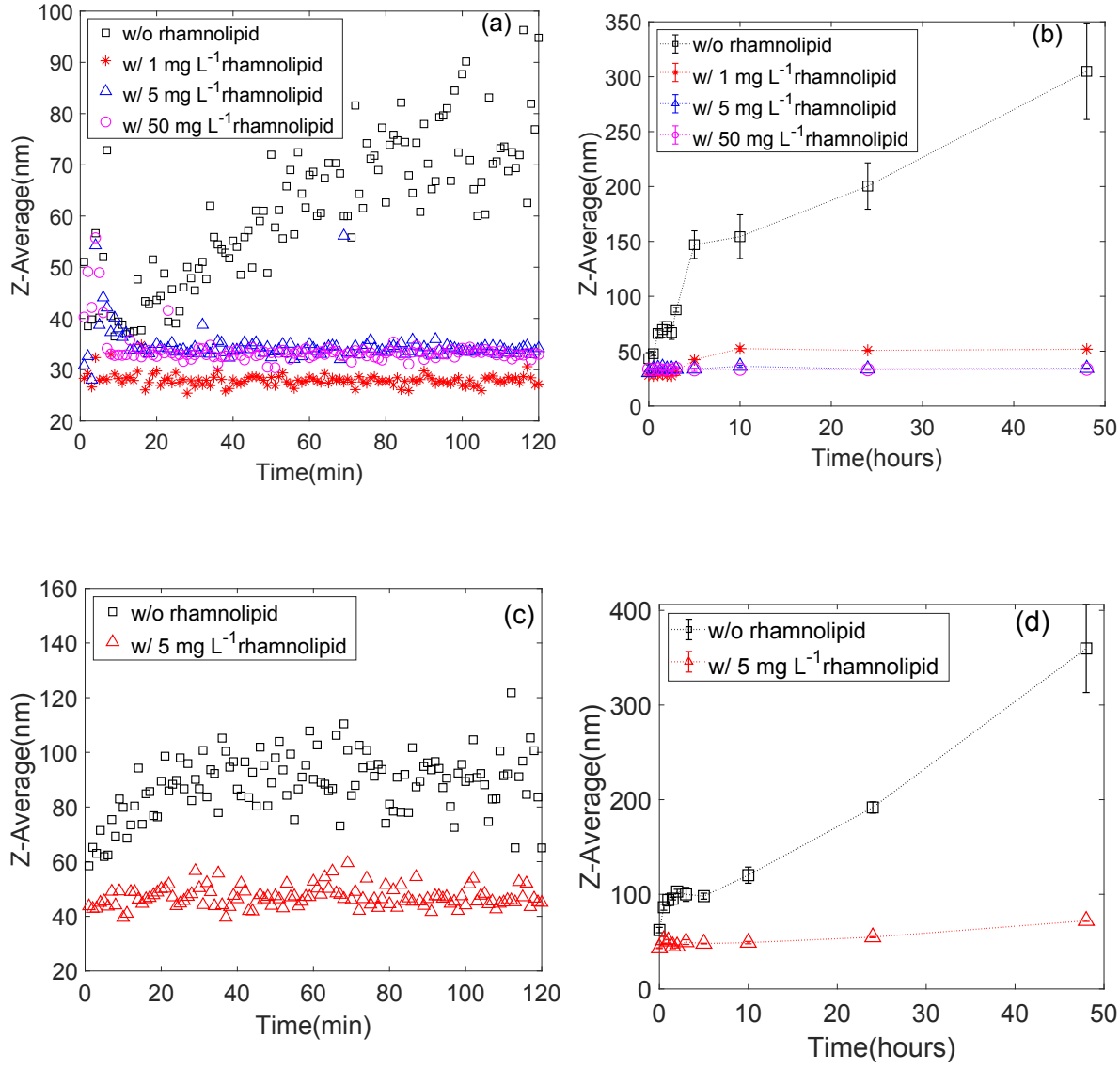

Figure S3. (a-b) nAg aggregation kinetics at pH 7.0±0.2 and dissolved oxygen concentration of 8.8±0.2 mg L^{-1} over 2 hours (short term) and 48 hours (long term). (c-d) nAg aggregation kinetics at pH 4.0±0.2 and dissolved oxygen concentration of 2±0.2 mg L^{-1} over 2 hours (short term) and 48 hours (long term). Error bars represent the standard deviation of duplicate/triplicate measurements.

4. nAg zeta potential and UV-Vis adsorption spectrum

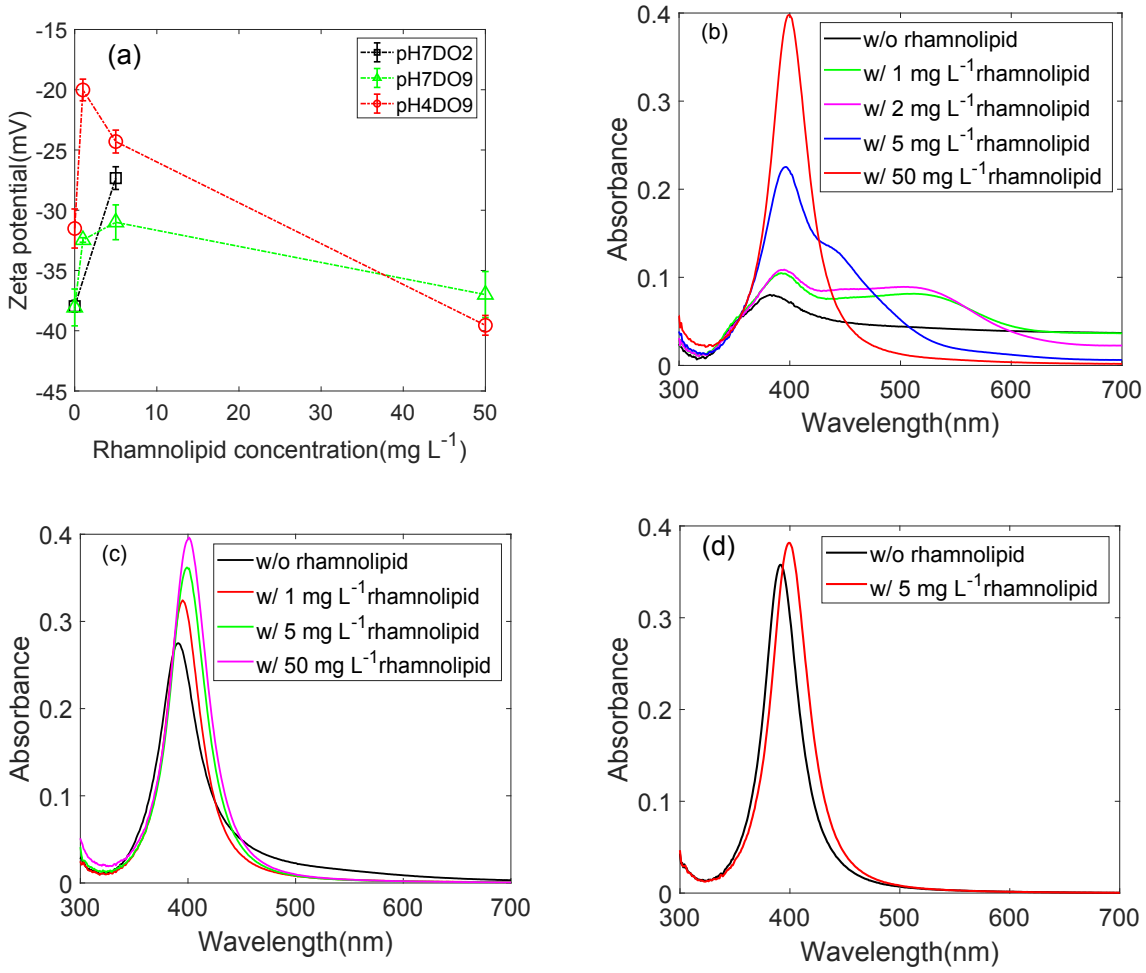

Figure S4. (a) nAg surface zeta potential under three pH and DO scenarios as a function of rhamnolipid concentration. (b-d) Absorption spectrum of nAg under three pH and DO scenarios as a function of rhamnolipid concentration.

5. nAg TEM images at pH = 7 and DO = 8.8 or 2.0 mg L^{-1}

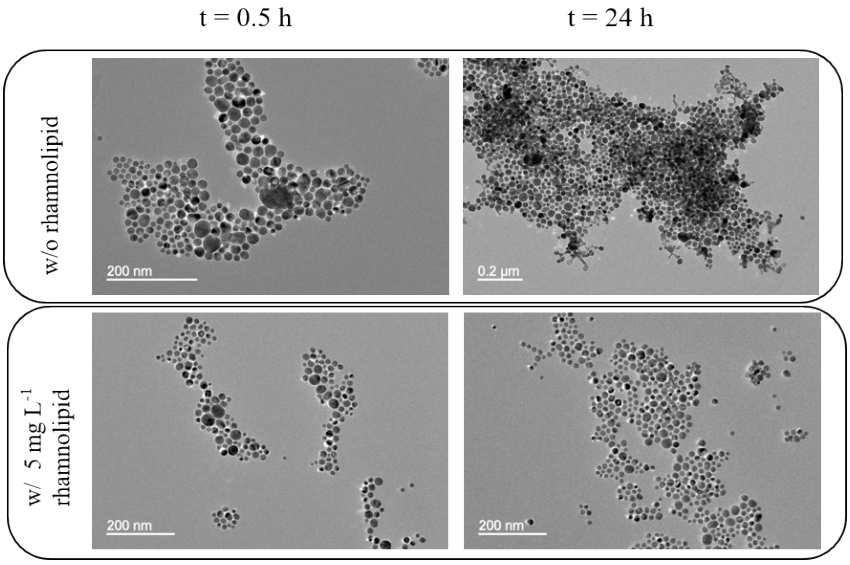

Figure S5. Representative TEM images of nAg (a) without rhamnolipid and (b) with 5mg L^{-1} rhamnolipid at 0.5 and 24 hours in aqueous solutions at pH 7.0 ± 0.2 and DO 8.8 ± 0.2 mg L^{-1}.

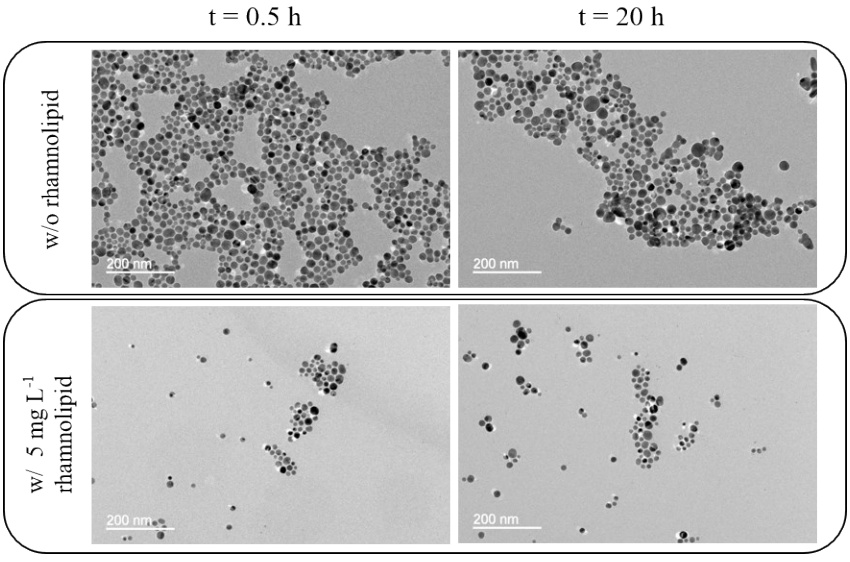

Figure S6. Representative TEM images of nAg (a) without rhamnolipid and (b) with 5mg L^{-1} rhamnolipid at 0.5 and 20 hours in aqueous solutions at pH 7.0±0.2 and DO 2.0±0.2 mg L^{-1}.

6. Energy profile calculations for nanoparticle-nanoparticle and nanoparticle-sand interactions

6.1. Nanoparticle-nanoparticle interactions

Derjaguin, Landau, Verwey and Overbeek (DLVO) theory[4, 5] can be used to evaluate the interactions between nanoparticles in varied solution chemistries. Based on DLVO theory, equations for calculations of Van der Waals interaction and electrostatic interactions are: [6, 7]

$$V_{VDW} = -\frac{A_H r}{12k_B T}[1 - \frac{bh}{\lambda} ln(1 + \frac{\lambda}{bh})] \qquad (S3)$$

$$V_{EDL} = 64\pi\varepsilon_0\varepsilon\frac{r}{2k_B T}(\frac{k_B T}{e})^2(tanh\frac{e\psi}{4k_B T})^2 \exp(-\kappa h) \qquad (S4)$$

Here, h is the distance between nanoparticles, b is a constant with a value of 5.32, λ is the characteristic wavelength for the interaction (100 nm), ε_0 is the permittivity of free space, ε is the dielectric constant of water, r is the nanoparticle radius, ψ is the ζ-potential of nanoparticles, κ^{-1} is the Debye-Hückel screening length, and A_H is the Hamaker constant for the nAg-water-nAg system, here 3.7E-20 J. [8] When rhamnolipid was present in the solution and absorbed on nanoparticle surfaces, steric repulsive interactions were also calculated based on equations presented in Fritz et al, [9] including osmotic interactions:

$$V_{OSM} = 0 \qquad 2d < h$$

$$V_{OSM} = \frac{4\pi r}{v_1}\psi^2(0.5 - \chi)\left(d - \frac{h}{2}\right)^2 \qquad d \le h < 2d$$

$$V_{OSM} = \frac{4\pi r}{v_1}\Phi^2(0.5 - \chi)d^2\left(\frac{h}{2d} - 0.25 - ln\frac{h}{d}\right) \quad h < d \qquad (S5)$$

and elastic repulsion:

$$V_{ELAS} = 0 \qquad d \le h$$

$$V_{ELAS} = (\frac{2\pi r}{M_W}\Phi d^2\rho_P)(\frac{h}{d}\ln\left(\frac{h}{d}\left(\frac{3 - \frac{h}{d}}{2}\right)^2\right) - 6ln\left(\frac{3 - \frac{h}{d}}{2}\right) + 3\left(1 + \frac{h}{d}\right)^2) \quad h < d \quad (S6)$$

Here, χ is the Flory-Huggins solvency parameter, which is assumed to be 0.286 for rhamnolipid, [10] Φ is the volume fraction of absorbed rhamnolipid within the brush layer, d is the thickness of the rhamnolipid brush layer, and v_1 is the volume of a solvent molecule. Φ was calculated based on the equation reported by Phenra et.al. [11] and d was estimated by the

size change measured by DLS at pH 7 and DO 9 mg L^{-1}. The resultant energy profiles are shown in Figure S7.

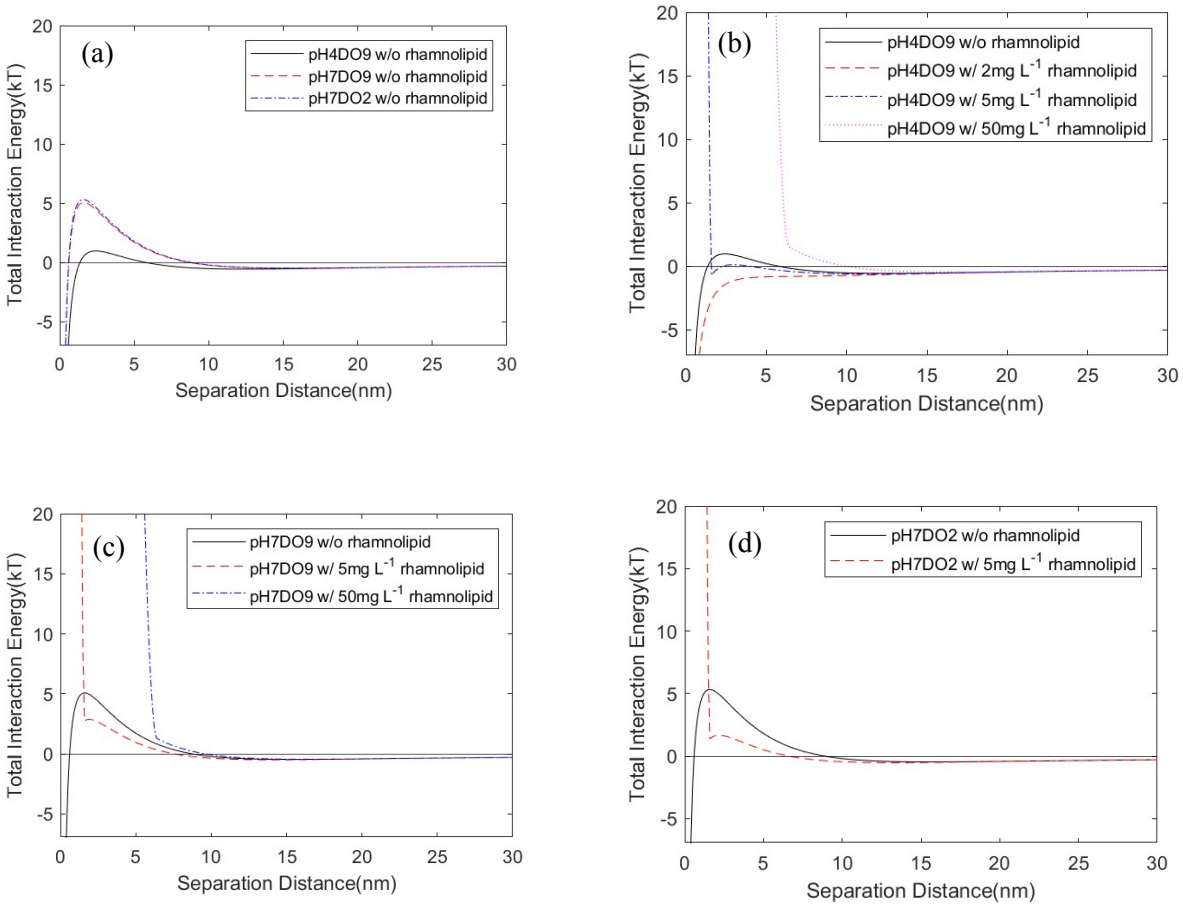

Figure S7. Interaction energy profiles between nAg particles under (a) three pH and DO scenarios; (b) for pH 4.0±0.2 and DO 8.8±0.2 mg L^{-1} with varying rhamnolipid concentrations in solution, (c) for pH 7.0±0.2 and DO8.8±0.2 mg L^{-1} with varying rhamnolipid concentrations in solution, (d) pH 7.0±0.2 and DO2.0±0.2 mg L^{-1} with varying rhamnolipid concentrations in solution. When rhamnolipid was present, steric repulsion was added to the total interactions and resulted a larger energy barrier.

6.2. Nanoparticle-sand interactions

DLVO theory can also be applied to the nanoparticle-sand interaction calculation. In this case, the double layer electrostatic repulsion and Van de Waals attraction between nanoparticle and sand surfaces were calculated as: [12, 13]

$$V_{EDL-ps} = \frac{\pi\varepsilon_r\varepsilon_0\kappa\left(\psi_s^2+\psi_p^2\right)}{k_BT}\int_0^a \left(-coth[\kappa(D+a-a\sqrt{1-\left(\frac{r}{a}\right)^2})]+coth[\kappa \right.$$
$$\left.)]+\frac{2\psi_s\psi_p}{\psi_s^2+\psi_p^2}\{csch[\kappa(D+a-a\sqrt{1-\left(\frac{r}{a}\right)^2})]-]-csch[\kappa(D+a+ \right.$$
$$\left.\sqrt{1-\left(\frac{r}{a}\right)^2})]]\})]\}\right)rdr \qquad (S7)$$

$$V_{VDW-ps} = -\frac{A_{ps}}{6}\left[\frac{a}{D}+\frac{a}{D+2a}+\ln\left(\frac{D}{D+2a}\right)\right] \qquad (S8)$$

Here, ψ_s and ψ_p are surface potentials of nanoparticles and sand grains, [14] respectively; D is the closest approach from nanoparticle to sand surface; a is the radius of nanoparticles; and A_{ps} is the Hamaker constant for nAg-water-quartz(silica) system, here 2.02E-20 J. [15]

Similar to the nanoparticle-nanoparticle interaction, the steric interaction energy (V_{S-ps}) can be calculated between a rhamnolipid-coated nAg and an uncoated sand grain[9, 10] and summed with the V_{EDL-ps} and V_{VDW-ps} values to obtain the total extended interaction energy:

$$V_{S-ps} = 0 \qquad d \le h$$

$$V_{S-ps} = \int_h^d 2\pi r\frac{k_BT}{s^3}\left(\frac{4L}{5}\left(\left(\frac{h}{d}\right)^{\frac{5}{4}}-1\right)+\frac{4L}{7}\left(\left(\frac{d}{h}\right)^{\frac{7}{4}}-1\right)\right)dD \quad h<d \quad (S9)$$

Here, s is the separation distance between rhamnolipid on the nanoparticle surface, which was estimated to be 0.68 nm, based on the nanoparticle surface area, average rhamnolipid molecular weight and rhamnolipid surface excess. The resulting interaction energy profiles based on these equations are shown in Figure S8.

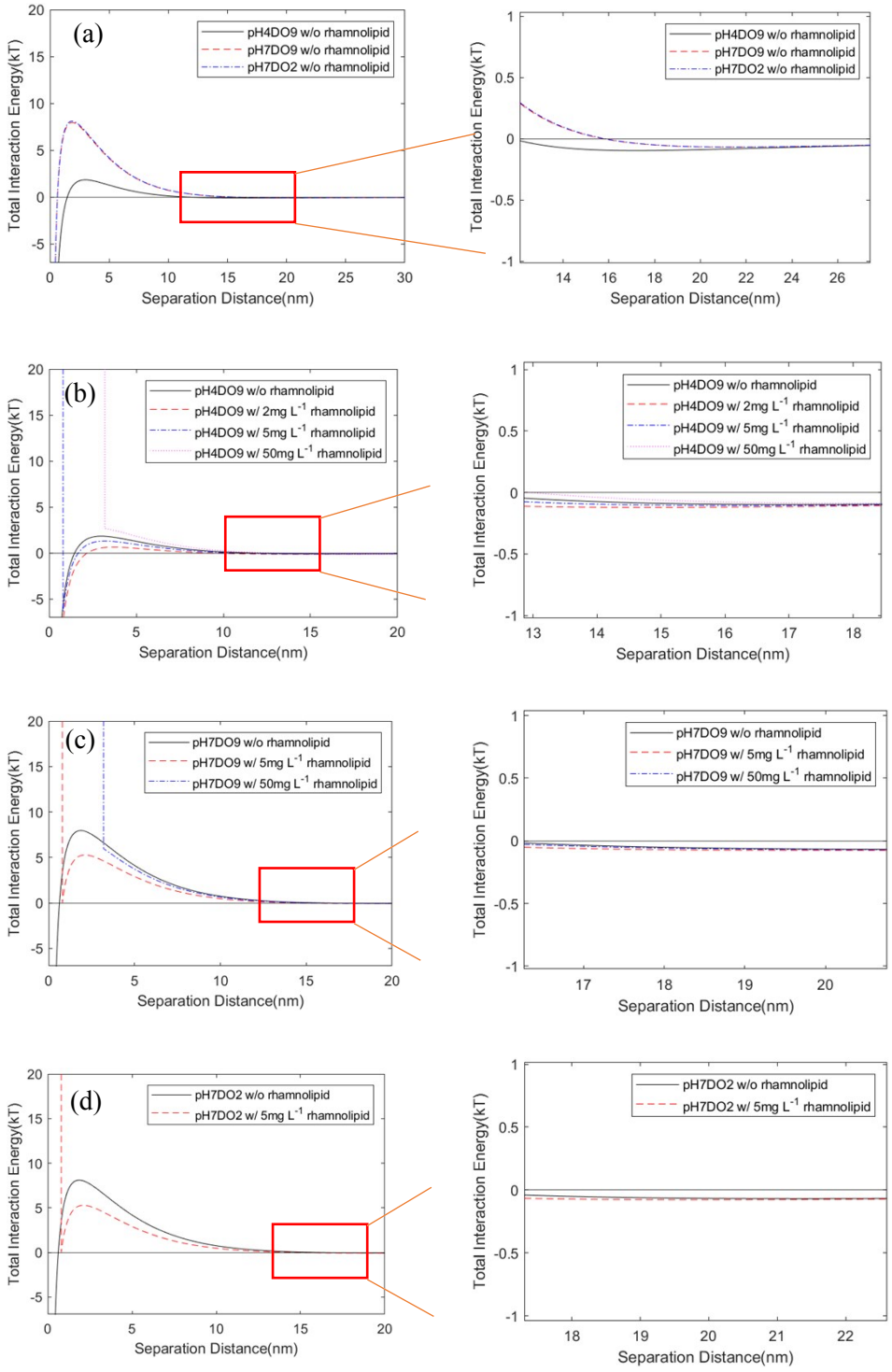

Figure S8. Interaction energy profiles for nAg and sand under (a) three pH and DO scenarios; (b) for pH 4.0±0.2 and DO 8.8±0.2 mg L^{-1} with a varying rhamnolipid concentration in solution, (c) for pH 7.0±0.2 and DO8.8±0.2 mg L^{-1} with a varying rhamnolipid concentration in solution, (d) for pH 7.0±0.2 and DO2.0±0.2 mg L^{-1} with a varying rhamnolipid concentration in solution. When rhamnolipid was present in the solution, steric repulsion was added to the total interactions and resulted a larger energy barrier. Figures in the second column are enlarged views of the secondary minimum region in Figures(a-d).

7. Energy-dispersive X-ray spectroscopy (EDS) analysis

Following SEM imaging, Energy-dispersive X-ray spectroscopy (EDS) analysis was conducted to confirm that the observed particles on the sand surface were silver nanoparticles (Figure 4c-d and Figure S9a, same sample with different magnifications). The electron acceleration voltage was 10 kV. The resulting elemental mapping and elemental spectroscopy of the sand surface (Figure S9a) are shown in Figure S9b-d and Figure S10, respectively. Three primary elements (silver, silica and oxygen) were detected on the sample surface and were labeled with different colors (Figure S9b-d): red, green and blue represent silver, silica and oxygen, respectively.

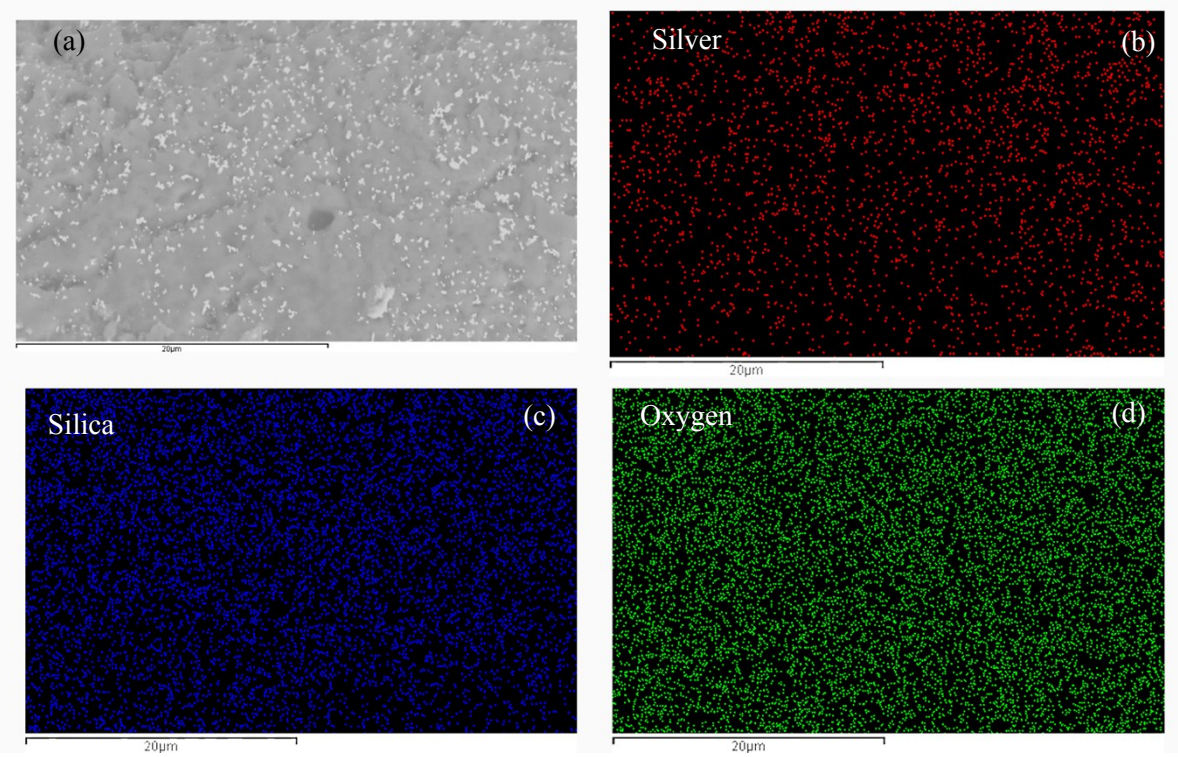

Figure S9. (a) SEM image of sand surface deposited with particles. (b-d) EDS elemental mapping of silver, silica and oxygen on the sand surface in (a), elements were labeled with different colors.

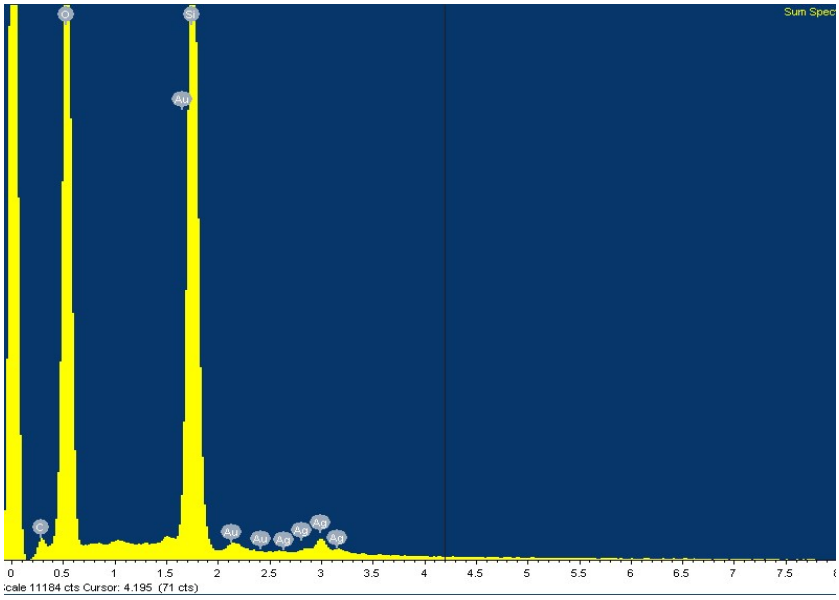

Figure S10. EDS spectroscopy of sand surface with deposited nAg in Figure S9a.

The amount of each element on the sand surface was obtained by analyzing the EDS spectroscopy and the results are presented in Table S2.

Table S2. Elemental weight and atomic percentages for nAg deposited on the sand surface (Figure S9a), obtained from elemental analysis of EDS spectroscopy (Figure S10).

Element	Weight%	Atomic%
C K	1.69	2.83
O K	54.94	69.14
Si K	37.89	27.16
Ag L	3.58	0.67
Au M	1.91	0.20
Totals	100.00	

References

1. N. Toride, F. Leij and M. T. Van Genuchten, The CXTFIT code for estimating transport parameters from laboratory or field tracer experiments, Version 2.1, Research Report No. 137, *Agricultural Research Service, US Department of Agriculture, Riverside, California*, 1995.
2. W. Zhang, Y. Yao, N. Sullivan and Y. Chen, Modeling the primary size effects of citrate-coated silver nanoparticles on their ion release kinetics, *Environ Sci Technol*, 2011, **45**, 4422-4428.
3. S. Kittler, C. Greulich, J. Diendorf, M. Köller and M. Epple, Toxicity of Silver Nanoparticles Increases during Storage Because of Slow Dissolution under Release of Silver Ions, *Chemistry of Materials*, 2010, **22**, 4548-4554.
4. B. Deraguin and L. Landau, Theory of the stability of strongly charged lyophobic sols and of the adhesion of strongly charged particles in solution of electrolytes, *Acta Physicochim: USSR*, 1941, **14**, 633-662.
5. E. J. W. Verwey, Theory of the stability of lyophobic colloids, *The Journal of Physical Chemistry*, 1947, **51**, 631-636.
6. T. Phenrat, N. Saleh, K. Sirk, R. D. Tilton and G. V. Lowry, Aggregation and sedimentation of aqueous nanoscale zerovalent iron dispersions, *Environ Sci Technol*, 2007, **41**, 284-290.
7. A. R. Petosa, D. P. Jaisi, I. R. Quevedo, M. Elimelech and N. Tufenkji, Aggregation and deposition of engineered nanomaterials in aquatic environments: role of physicochemical interactions, *Environ Sci Technol*, 2010, **44**, 6532-6549.
8. K. A. Huynh and K. L. Chen, Aggregation kinetics of citrate and polyvinylpyrrolidone coated silver nanoparticles in monovalent and divalent electrolyte solutions, *Environ Sci Technol*, 2011, **45**, 5564-5571.
9. G. Fritz, V. Schädler, N. Willenbacher and N. J. Wagner, Electrosteric stabilization of colloidal dispersions, *Langmuir*, 2002, **18**, 6381-6390.
10. J. Xu, S. Sun, Z. Wang, S. Peng, S. Hu and L. Zhang, pH-Induced evolution of surface patterns in micelles assembled from dirhamnolipids: dissipative particle dynamics simulation, *Phys Chem Chem Phys*, 2018, **20**, 9460-9470.
11. T. Phenrat, N. Saleh, K. Sirk, H.-J. Kim, R. D. Tilton and G. V. Lowry, Stabilization of aqueous nanoscale zerovalent iron dispersions by anionic polyelectrolytes: adsorbed anionic polyelectrolyte layer properties and their effect on aggregation and sedimentation, *Journal of Nanoparticle Research*, 2007, **10**, 795-814.
12. S. Bhattacharjee and M. Elimelech, Surface element integration: A novel technique for evaluation of DLVO interaction between a particle and a flat plate, *Journal of Colloid and Interface Science*, 1997, **193**, 273-285.
13. K. A. Guzman, M. P. Finnegan and J. F. Banfield, Influence of surface potential on aggregation and transport of titania nanoparticles, *Environ Sci Technol*, 2006, **40**, 7688-7693.
14. Y. Wang, H. Zhu, M. D. Becker, J. Englehart, L. M. Abriola, V. L. Colvin and K. D. Pennell, Effect of surface coating composition on quantum dot mobility in porous media, *Journal of Nanoparticle Research*, 2013, **15**.
15. A. M. Mittelman, *The effects of surface aging on nanoparticle fate and transport in natural and engineered porous media*, PhD, Tufts University, 2015.